Biomechanical properties and resistance to uprooting of laboratoryscale wood logs

Biomechanical properties and resistance to uprooting of laboratory-scale wood logs

Valentina Bau'[1], **Paolo Perona** [1]

[1]Institute for Infrastructure and Environment, School of Engineering, The University of Edinburgh, Edinburgh, UK

Key Points:

- Wood log growth experiments reveal uniform distribution of root biomass along the trunk
- Uprooting tests show linear and nonlinear dependencies of mechanical anchoring on root biomass
- Survival to uprooting by flow of young rejuvenated wood logs occurs within windows of opportunity

Corresponding author: Valentina Bau', v.bau@ed.ac.uk

Abstract

Wood dynamics affects riparian ecosystem functioning and river morphology. The spatial and temporal dynamics of wood pieces in river corridors, in particular of deposited rejuvenated wood logs, depend on their biomechanical properties and resistance to uprooting. The ability of stranded wood logs to withstand drag forces depends on how efficiently their roots have sprouted and on the interarrival time, magnitude, and duration of the moderate floods to which they are subjected. We performed static pullout tests on small-scale wood logs (*Salix* species) of 4 different sizes, growth stages, and sediment moisture content. Statistics of root biomass growth rate and related spatial distribution along the trunk reveal important insights for upscaling dynamics. Similarly, force-displacement curves indicate the maximum resistance and related energy for uprooting. Autocorrelation analysis of the sequence of force drops in the force-displacement signal reveals the statistical nature of the mechanism of load redistribution among roots. These results are then used to advance a physically-based mathematical model of the resistance of wood log roots to flow-induced drag forces. Given that the magnitude, duration, and return period of hydrologic events are typically correlated, our model implies the existence of windows of opportunity for wood logs to either survive or re-mobilize.

1 Introduction

Riparian zones are defined as complex transitional ecotones occurring between terrestrial and river ecosystems [*Gregory et al.*, 1991; *Malanson*, 1993; *Gurnell et al.*, 1995; *Tabacchi et al.*, 1998; *Naiman et al.*, 2005]. Within riparian zones, the hydrological, geomorphic, and ecological processes interact over wide spatial and temporal scales and contribute to bidirectional exchanges of energy and material [*Likens and Bormann*, 1974; *Johnston and Naiman*, 1987; *Bendix and Hupp*, 2000; *Hungr et al.*, 2001; *Steiger et al.*, 2005; *Wilford et al.*, 2005; *Pinay et al.*, 2018]. A key material exchange between rivers and adjacent riparian areas involves the transfer of wood logs to stream channels [*Latterell et al.*, 2006; *Naiman et al.*, 2000; *Gurnell et al.*, 2005; *Wohl*, 2019], a process that often takes place after high magnitude flooding events [*Mao et al.*, 2013; *Comiti et al.*, 2016; *Ruiz-Villanueva et al.*, 2016; *Zischg et al.*, 2018]. The presence of wood material has been recognised to be as fundamental a component of woodland fluvial ecosystems as sediment and riparian vegetation [*Anderson et al.*, 1978; *Abbe and Montgomery*, 1996; *Gurnell et al.*, 2002; *Gregory et al.*, 2003; *Tockner et al.*, 2003; *Seo and Nakamura*, 2009; *Beckman and*

Wohl, 2014; *Wohl and Scott*, 2017]. Wood accumulations may have an impact on flow resistance, affecting the pattern and geomorphology of rivers [*Young*, 1991], and local sedimentation and erosion processes [*Gippel et al.*, 1996; *Grunell*, 1997; *Brooks and Brierley*, 2002]. Besides providing a niche for aquatic and terrestrial lifeforms [*Fisher and Likens*, 1972], wood accumulations may also hinder the downslope transfer of both organic materials and nutrients and promote their retention [*Thompson*, 1995]. As a result, wood logs may act as ecosystem and geomorphological engineers by initiating island nuclei, sustaining water quality, providing nutrients and shelter for organisms, and creating a variety of physical habitats [*Décamps and Naiman*, 1990; *Naiman and Decamps*, 1997; *Francis et al.*, 2008; *Corenblit et al.*, 2011; *Welber et al.*, 2012; *Gurnell et al.*, 2001].

The motion of wood logs in rivers involves three steps: recruitment, transport, and deposition [*Gasser et al.*, 2019]. Recruitment is a combination of selection and delivery mechanisms of wood logs from river bedforms and banks into streams, and is triggered by stochastic geophysical events such as hillslope failure [*Keller and Swanson*, 1979; *Nakamura and Swanson*, 1993; *Comiti et al.*, 2016; *Cadol et al.*, 2009; *Rigon et al.*, 2012; *Iroumé et al.*, 2015], bank erosion [*Sedell and Froggatt*, 1984; *Gurnell et al.*, 2000; *Downs and Simon*, 2001; *Moulin and Piégay*, 2004; *Lassettre et al.*, 2008; *Ulloa et al.*, 2015], snow avalanches [*Bebi et al.*, 2009], and stand-replacing events (e.g. tree windthrow [*Welty et al.*, 2002] and wild fires [*Benda et al.*, 2003; *Rosso et al.*, 2007]). Transport refers to the mobilization of wood logs in river corridors. This is also influenced by river morphology, first-order control on the wood regime [*Wohl*, 2019], and wood properties (e.g., orientation, size, and density) [*Gurnell et al.*, 2002; *Braudrick and Grant*, 2000; *Wohl*, 2011; *Ruiz-Villanueva et al.*, 2016]. Finally, deposition is the process by which wood logs settle on floodplains and alluvial bedforms, such as bars and islands, as a result of low flow conditions or narrowing of the river section [*Gasser et al.*, 2019]. Deposition of wood in rivers has been widely observed and its important ecological functions studied in detail, including maintenance of aquatic and terrestrial habitats and provision of food resource for aquatic organisms [*Gregory et al.*, 2003; *Gurnell and Petts*, 2006]. The deposition of wood pieces on river bedforms, and their interactions with river processes are believed to play an important role in the geomorphic complexity and ecological diversity of rivers [*Montgomery et al.*, 2003; *Gurnell et al.*, 2005; *Francis*, 2007; *Gurnell et al.*, 2012; *Ruiz-Villanueva et al.*, 2016]. Notably, this is also influenced by the ability of many riparian wood species to re-sprout and develop adventitious roots once deposited, thus leading to

the emergence of pioneer landforms [*Gurnell et al.*, 2005]. For example, river bars in the Tagliamento river were found to be significantly affected by the regeneration of driftwood [*Gurnell and Petts*, 2002; *Francis and Gurnell*, 2006]. Species that can resprout and regrow invariably reproduce vegetatively. For instance, in a study of the riparian forests of the Pacific Coastal Ecoregion, *Naiman et al.* [2000] report that redwood, willow, poplar, and ash are notable examples of species likely to develop roots from disseminated fragments. *Karrenberg et al.* [2002] also observed that *Salicacae* species can re-sprout vigorously from deposited vegetative fragments. Figure 1 shows three examples of wood fragments resprouting and rooting again, after deposition on moist sediment.

Meanwhile, the successful sprouting and establishment of roots from rejuvenated wood-logs on river bedforms depends on the resistance of roots to remobilization or uprooting by flow, which is determined by the biomechanical properties of the root-soil architecture [*Edmaier et al.*, 2011]. *Edmaier et al.* [2011] found that the mechanism of plant uprooting by flow can occur almost instantaneously (uprooting of Type I) when plants are in their early stage of growth or as a time delayed process (uprooting of Type II) when flow-induced drag and bed erosion processes exceed the anchoring resistance exerted by the root system, as confirmed by *Bywater-Reyes et al.* [2015] in a field setting. Substantial research has been devoted to understanding the dynamics of recruitment and transport [*Braudrick et al.*, 1997; *Bocchiola et al.*, 2002; *Daniels*, 2006; *MacVicar and Piégay*, 2012; *Iroumé et al.*, 2015; *Ravazzolo et al.*, 2015; *Ruiz Villanueva et al.*, 2014; *Martin and Benda*, 2001], but has not yet explored the biomechanical properties and root resistance of deposited regenerating wood logs. From this perspective, the biological timescale becomes fundamentally important because the mechanism of remobilization of wood logs results from competition dynamics between the plant biological growth rate and the frequency and magnitude of flood disturbance. Therefore, knowledge of the biomass developed by resprouted wood logs at different timescales and quantification of the respective rooting anchoring resistance would facilitate assessment of the roots' ability to withstand water drag forces. However, assessment of the biomechanical properties of wood logs in situ is not an easy task, owing to several constraints that make wood deposition and remobilization processes difficult to monitor. For instance, depending on the obstacle-to-sediment size ratio, scour and deposition processes may have a significant influence on remobilization of wood logs. However, tracking river processes in field-scale experiments is difficult

to achieve. Therefore, it is necessary to investigate the resilience of wood logs by undertaking controlled laboratory experiments.

The aim of this paper is to study the growth dynamics of small-scale wood logs and explore their mechanical resistance through pullout experiments. Vertical uprooting experiments that measure root pulling-out resistance provide the most efficient way to determine the root anchorage of a plant [*Ennos and Pellerin*, 2000]. Rooting resistance is typically quantified by means of force/extension curves related to parameters that express root architecture (such as root length and root diameter) [*Edmaier*, 2014; *Bywater-Reyes et al.*, 2015; *Bankhead et al.*, 2017; *Karrenberg et al.*, 2003]. This approach provides insights into the complex dynamics of deposition and remobilization of wood logs in rivers.

In this work, 326 plant uprooting tests involving logs of different sizes were successfully performed for two different sediment moisture contents and at different growth stages. The prototype plant comprised wood cuttings (*Salix* species), which served as a surrogate for small wood logs. Cuttings of four different sizes were tested in order to advance upscaling rules that will enable the biomechanical properties of *Salix* wood logs to be reproduced correctly at field scale. Architectural parameters, including below-ground biomass (e.g., root length) and above-ground biomass (e.g., branch size) were computed in order to estimate the flow-induced drag force on a wood log when subjected to the stream velocity during a certain flooding event. This enabled us to back-calculate the magnitude and the return time of hydrologic events that may remove rejuvenated logs at early stages of growth, depending on the relative elevation of sites where logs are deposited. The understanding gained from the present results will help improve deterministic and stochastic models for riverbed vegetation dynamics (e.g. encroachment, deposition, persistence, remobilization) and to inform river restoration and management projects.

2 Material and methods

2.1 Material and experimental setup

The cuttings used in the present experiments were harvested from a single *Salix fragilis* located on the riverbanks of the Braid Burn, close to the King's Building campus in Edinburgh. This species is a member of the *Salicacae* family, which have a high capacity to sprout roots when fragments are exposed to adequate moisture conditions (e.g. *Tyce* [1957]) and reproduce freely from cuttings or broken branches [*Howell et al.*, 1994].

Figure 1. Examples of regrowth stages of wood logs of different sizes that have sprouted on river bars: a) sprouting of a willow branch from a log deposited on a bar in the Sense River, Switzerland (photograph courtesy of V. Ruiz-Villanueva); b) deposited wood fragments on a bar in the Thur River, Switzerland (photograph: P. Perona) where it can be deduced from the stage of evolution of the branches that the root system of the logs may have developed a certain anchoring resistance; and c) example of sprouting from below ground.

Furthermore, the use of cuttings rather than seedlings allowed processes that occur widely in nature to be simulated, given that wood fragments deposited on river bedforms mainly derive from broken branches or trunks of trees transported during floods. In addition, the cuttings reproduce, at small scale, a tree trunk or wood log and facilitate the design of an upscaling procedure. Each cutting was assigned randomly to rhizoboxes and was planted horizontally, half-embedded in washed mineral sand with a mean grain size of $\sim$ 1 mm. This sediment size class is often found on river bars and islands (e.g. see *Moggridge* [2007]; *Pasquale et al.* [2011]). However, it should be noted that use of sand on its own may not be fully representative of the variability of the sediment calibre encountered on the surface (and subsurface) of sediment patches. Even so, sand can be useful as an idealised prototype soil medium in which to test plant uprooting resistance at laboratory scale (e.g. see *Edmaier* [2014]; *Calvani et al.* [2019]). The sediment depth was set equal to 16 cm in order to avoid root growth being constrained by the bottom of the box. Rhizoboxes are permeable to water and so were placed inside a bigger plastic container filled with water. In this way the water table was maintained at a level of 6 cm below the soil surface leading to the formation of an unsaturated zone of 60% relative moisture content through capillary rise (Figure 2a). Cuttings were pruned into four different standard lengths L: 5, 10, 15 and 20 cm. The resultant mean diameter of all collected samples, $\bar{d}$, was 1.20 cm, with a standard deviation, σ, equal to 0.2. Cuttings were allowed to grow roots and stems before being uprooted. The lower time limit of growth for the plant to be uprooted was set to 2 weeks in order to allow the roots to develop a certain resistance after sprouting.

166 The maximum growth time was 9 weeks (see Table 1). The upper growth limit was dic-
167 tated by the state of health of the plant: it has been observed that after 60 days, plants
168 were likely to weaken and die. For most alpine rivers, this timescale corresponds to the
169 return period of small to moderate floods able to remobilize the logs [*Trush et al.*, 2000].
170 No nutrient solution was used to accelerate the growth of the plants. On average, every 4
171 days, the following measurements were taken for each cutting: living/dead status, number
172 of stems and their combined length, and the number of living leaves. The measurements
173 were carried out throughout the lifetime of the plants using a simple ruler (precision 0.1
174 cm). The temperature in the laboratory had a mean value of 22°C and a maximal diurnal
175 fluctuation of 4°C. Once cuttings had reached their specified growth duration, they were
176 extracted from the soil using a motorized pulley system similar to that of *Edmaier et al.*
177 [2014] (Figure 3a). For certain samples, the uprooting was obtained under the same mois-
178 ture conditions as during the growth phase (60% soil moisture) (Figure 2a), whereas for
179 the remaining samples, the water table level was raised to the sediment surface creating a
180 saturated medium (Figure 2b). This latter scenario is more representative of conditions to
181 which pioneer plants are subjected, and it enables determination of the sediment moisture
182 condition applicable to plant uprooting in rivers. Although vertical pullout tests lead to
183 overestimation of the root resistance [*Coutts*, 1983], these tests were nevertheless deemed
184 sufficiently reliable to quantify the force required to break the soil-root friction, which,
185 when the plant is flexible, is unaffected by the direction of pull [*Bankhead et al.*, 2017]. It
186 should be noted that water table fluctuations were not taken into account in these exper-
187 iments. Based on the literature (e.g. *Francis et al.* [2005]; *Hughes et al.* [1997]; *Guilloy*
188 *et al.* [2011]) and on the control that the water table level exerts on the balance between
189 oxygen and water in the soil, it is obvious that the use of different water table depths
190 would have affected the biomass evolution of the cuttings, thus adding a further variable
191 to the problem.

192 **Table 1.** Summary table listing the length of the cuttings tested, uprooting time, and the total number of
193 samples pulled out. Uprooting time refers to the elapsed time between when a cutting is laid on the sediment
194 and when it is uprooted.

cutting size [cm]	**uprooting time [weeks]**	**total samples**
5, 10, 15, 20	2, 3, 4, 5, 6, 7, 8, 9	326

2.2 Uprooting Experimental procedure

The plant-wire connection system (Figure 3b) was designed to apply direct traction. To achieve this, both extremities of the cutting were clipped to a double loop nylon wire. The loops were tied by means of two drawing pins that had been fixed into the extreme cross-sections during the planting stage to avoid disturbing the later anchorage of the plant. Cuttings were pulled up at constant vertical velocity (1.71 mm/s) by a computer-controlled motor-encoder (EPOS), enabling measurment of the force fluctuations induced by the root system. The vertical uprooting force was recorded at 100 Hz by a piezoelectric force sensor (Kistler) calibrated with a force range of ±50 N. The output load cell signal was routed directly to an external charge amplifier (Kistler) that produced an output voltage signal proportional to the mechanical stress (Figure 3a). Measurements of the root architecture parameters were recorded immediately after the samples were uprooted, to avoid inaccuracy from changes to the roots as they lost water content. Roots were gently detached from the log and washed to remove residual soil particles, and then scanned using a EPSON Expression 10000 XL (optical resolution: 2400 dpi). Starting from a predetermined reference point, the relative position of each root along the cutting was assigned an appropriate interval of 1 cm. The small magnitude of the intervals improved the accuracy of the estimated amount of biomass that had grown along the cutting. The root architecture parameters (i.e. root length, volume, surface area) were computed using WinRHIZO BASIC 2009 root analysis software (Régent Instruments Canada, Inc.) for the total root biomass present in each interval.

2.3 Statistical analysis

The evolution of the plant biomass was evaluated in terms of sample averages, whose values were fitted to extrapolate growth laws for parameters representing below- and above-ground biomass. Computation of the averages of the root length, number of roots, root surface area, and stem length was undertaken for samples of the same size uprooted within the same week. Trends in average root depth (the average ratio between length and number of roots) and other allometric laws were obtained regardless of the size of the cuttings. A one-sample Kolmogorov-Smirnoff test was carried out to assess whether the observed data on root biomass were uniformly distributed over the normalised cutting lengths. For plants that developed stems (about 65% of the total samples), averaged measurements of

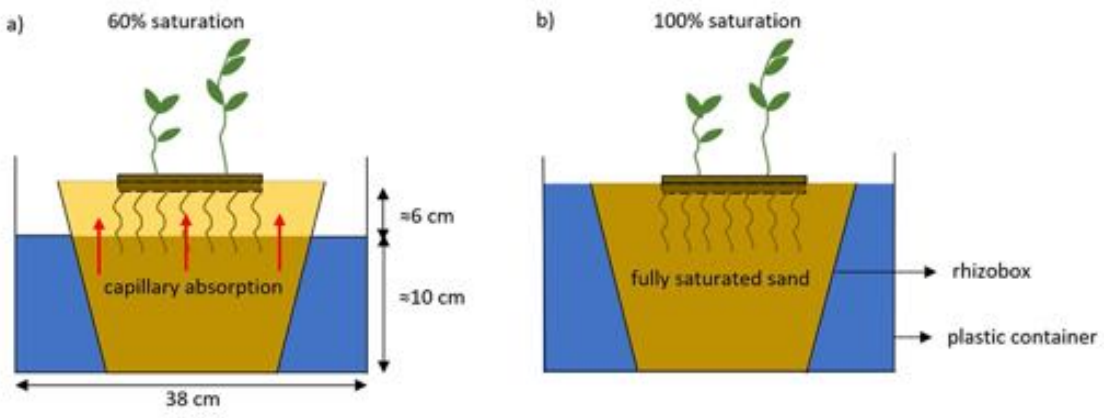

196 **Figure 2.** Sketches of the containers used in the experiments. The plastic box containing the sediment (rhi-
197 zoboxes) is stored inside a plastic container filled of water. The rhizoboxes are non-water tight. a) The water
198 level is kept about 6 cm below the sediment surface, corresponding to 60% relative moisture of the unsatu-
199 rated layer. (This setting was applied to the growth phase of all the plants); b) Soil moisture conditions when
200 the samples were uprooted. To achieve 100% saturated soil, the water table level was raised to the surface of
201 the sediment.

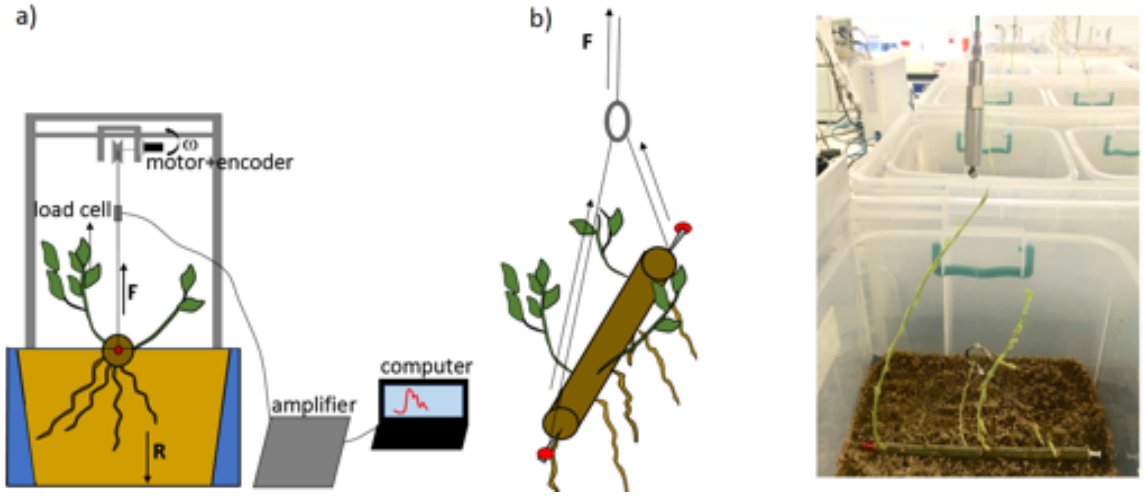

222 **Figure 3.** Sketch of the pull-out experiment. a) Motorized pulley system whereby the cutting is uprooted
223 by an external force powered by a motor whose rotation was measured by an encoder. The exerted force **F**
224 was continuously recorded by a load cell attached to an amplifier that was connected in turn to a computer.
225 The modulus of **F** is equal to the anchoring resistance **R** developed by the root system; b) Schematic view and
226 photograph of the plant-wire connection system.

total stem length and number of leaves were also computed. Samples that died were discarded from the statistics, along with plants that did not develop any root system.

Sample statistics were obtained of the force drops, and their sequence autocorrelation extracted from the uprooting curve. Similar procedures were applied to the sequence of intertime values between consecutive force drops. This facilitated characterization of the statistical nature of the load redistribution mechanism among roots in soil with two different values of moisture content.

2.4 Drag force model and uprooting by flow

The likelihood of a wood log to experience flow-induced drag and hence possibly be removed depends on the topographic elevation above the water level at which the log was deposited in relation to the duration and the magnitude of a given flooding event. By determining the stream velocity, u, at a given location and the projected area of the log, it is then possible to compute a value for the flow-induced drag force at which plant removal would occur. In the present computation, we assume a worst-case scenario where the impact between the longitudinal cross section of the log and the flow is perpendicular. The force components acting on a submerged plant were evaluated following the approach proposed by *Bau et al.* [2019], whereby the drag force, $\mathbf{F_d}$, is given by the sum of normal $\mathbf{F_{d,n}}$ and tangential $\mathbf{F_{d,t}}$ force components, such that

$$\mathbf{F_d} = \mathbf{F_{d,n}} + \mathbf{F_{d,t}} \tag{1}$$

The modulus of $\mathbf{F_{d,n}}$ is:

$$F_{d,n} = \frac{1}{2} C_d \rho_w u^2 A_n, \tag{2}$$

where C_d is the drag coefficient, u is the approach flow velocity impacting the log and A_n the projected area of the trunk of the log in the flow direction. The modulus of $\mathbf{F_{d,t}}$ was calculated as:

$$F_{d,t} = \frac{1}{2} C_f \rho_w u^2 (A_s + A_l), \tag{3}$$

where C_f is the friction coefficient, A_s is the total surface area of the stems, and A_l is the total area of the leaves exposed to the flow. To calculate the projected and surface areas A_n, A_s and A_l, the trunk, stem, and leaves were approximated by simple geometric shapes: a rectangle, a cylinder, and rhombus, respectively (see *Bau et al.* [2019]). C_d and C_f were each assigned a representative value of 1 [*Järvelä*, 2002].

3 Results

3.1 Below- and above-ground biomass

The scanned image of a generic cutting after uprooting (Figure 4a) shows that the root biomass per unit length, $\omega(x)$, is almost uniformly distributed over the distance coordinate x. This observation is confirmed by considering the variation in normalized cumulative sum of the total root surface area, $\Omega(\tilde{x}) = \int_0^{\tilde{x}} \omega(\xi) d\xi$, with normalised cutting length, $\tilde{x} = \frac{x}{L}$ (Figure 4b). The normalised cumulative sum profiles shown in Figure 4b are plotted for all growth stages and all cutting sizes. Results from the one-sample Kolmogorov-Smirnoff test showed that the null hypothesis was never rejected for a significance level equal to 0.05, implying that the empirical distribution functions are statistically close to the uniform density distribution. This indicates that the logs tend to develop roots at a constant spatial distance independent of their size, which is relevant for upscaling purposes. Figure 5a summarizes the growth statistics obtained for the different cuttings. Figure 5a shows that the growth trends of the root lengths tend to follow power laws of the form $\bar{L}_r = c_1 \cdot t^{d_1}$. Similar trends emerge in Figure 5b, which depicts the variation in

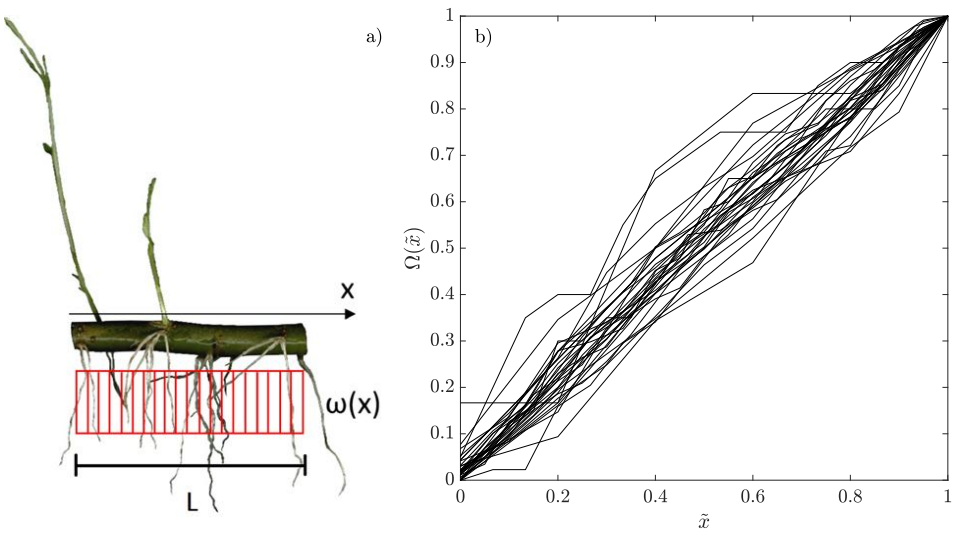

Figure 4. a) Coloured scanned image of a sample of length L. (red bars highlight the uniform distribution of the root biomass over the distance coordinate x); b) normalized cumulative sums of the total root surface area of the samples versus normalized cutting length.

averaged number of roots, $\bar{n}_r$, with time. Average values of the number of roots were calculated following the same approach used for the total root length, and the results fitted to equations of the form: $\bar{n}_r = c_2 \cdot t^{d_2}$. Table 2 lists the fitting coefficients and the goodness of fit measures, R^2, for both power laws. After determining $\bar{L}_r$, $\bar{n}_r$, and the uniform distribution of the roots with x (Figure 4), it was then possible to evaluate the average root depth, $\bar{l}$. Once again, the power law is most suitable to describe the trend in average root depth over time: $\bar{l} = c_3 \cdot t^{d_3}$ (Figure 5c). Table 3 lists the resulting values for c_3 and d_3. Figure 5d shows the variation of the averaged total length of the stems, $\bar{L}_s$, with time for each size class. The trend followed by the data points suggests that a logistic curve would be suitable to describe plant growth limited by carrying capacity, here represented by the internal nutrient reserves of the wood log [*Schimpf et al.*, 1977; *Hsu et al.*, 1984]. The logistic curve for averaged total length of stems is:

$$\bar{L}_s(t) = \frac{\bar{L}_{s,max}}{1 + e^{-b(t-t_0)}} \tag{4}$$

where $\bar{L}_{s,max}$ is the curve's maximum value which coincides with the averaged total stem length recorded in the last growth range, b is the logistic growth rate and t_0 is the location of the midpoint of the sigmoid. To achieve the best fit, the value of b was set equal to 0.12 independent of L, t_0 was located at 28 for both L=5 cm and L=20 cm, and at 30 and 27 for L=10 cm and L=15 cm, respectively. The equation predicted that stems grow to a maximum value corresponding to the carrying capacity of the logistic model. The maximum average total stem length generally increases progressively with L, the size of the cutting (Figure 5d), except for plants with L=10 cm, whose maximum value is slightly above that reached by plants of size 15 cm, possibly due to experimental noise effects. Figure 5e displays how the average number of leaves $\bar{n}_l$ correlates linearly with $\bar{L}_s$. Here data are fitted by a regression line of the form: $\bar{n}_l = c_4 \cdot \bar{L}_s$. Figure 5f shows the correlation between the total length of the stems and the total root volume developed by the time of uprooting. However, owing to the high variability of data, the stem length and the root volume were represented by mean values, $\bar{L}_s$ and $\bar{V}_r$, computed for all samples at the same growth stage. In this case, data follow a power law with equation: $\bar{L}_s = c_5 \cdot \bar{V}_r^{d_5}$. A similar fitting law was also obtained in a previous experimental study [*Pasquale et al.*, 2014]. Table 3 lists the fitted coefficients for $\bar{n}_l$ and $\bar{L}_s$.

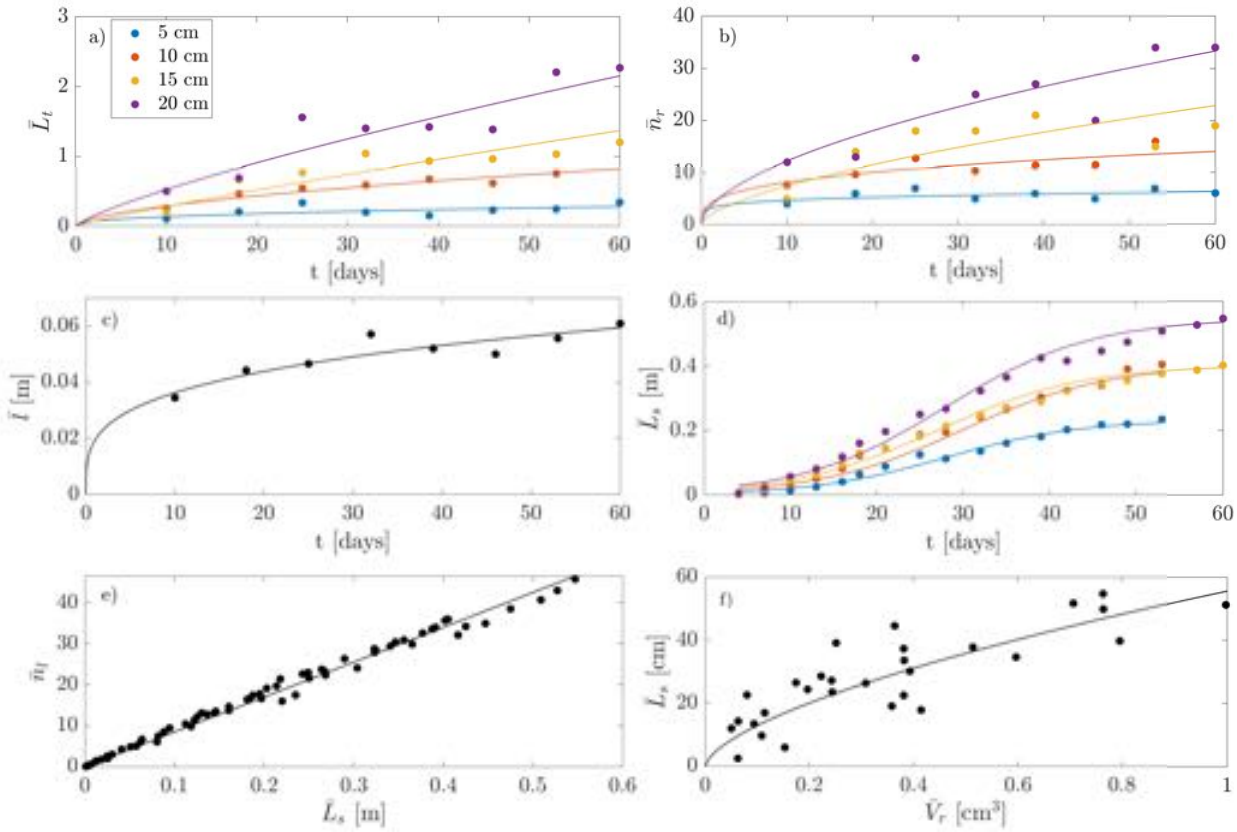

Figure 5. Average trends in below-ground parameters: a) variation in average total root length with time for different size of cuttings; b) variation in average root number with time for different sizes of cuttings; c) variation in average root depth over time; d) trends in average value of the total stem length with time for each cutting size; e) average number of leaves with averaged total length of the stems; and f) average total stem lentgh versus averaged root volume.

3.2 Resistance to uprooting

The force-displacement signals illustrated in Figure 6 show the anchorage ability of roots to withstand a vertical pulling force. In general, the force-displacement curve comprises three main phases, as identified in previous studies [*Edmaier et al.*, 2011; *Ennos*, 1989]. The first phase is a non-linear elastic phase, during which the force increases non-linearly with elastic recovery. The second phase presents linear elastic behaviour until maximum uprooting resistance is achieved. This quantity corresponds to the highest value of the tensile force that the root system can withstand. The third phase is the descending process, where the force decline occurs as a sequence of drops and partial elastic recoveries until uprooting is entirely achieved. This last phase is the result of the progressive

316 **Table 2.** Fitting coefficients and goodness of fit R^2 for power laws fitting $\bar{L}_r$ and $\bar{n}_r$.

	$\bar{L}_r$ [m]			$\bar{n}_r$ [-]		
cutting size	c_1	d_1	R^2	c_2	d_2	R^2
5 cm	0.05	0.41	0.41	3.19	0.17	0.28
10 cm	0.08	0.58	0.92	4.08	0.30	0.64
15 cm	0.04	0.88	0.81	1.78	0.62	0.69
20 cm	0.08	0.81	0.88	3.38	0.56	0.66

317 **Table 3.** Fitting coefficients and goodness of fit R^2 for power laws fitting $\bar{l}$ and $\bar{L}_s$ and the linear law fitting
318 $\bar{n}_l$. For these parameters, the fitting equations are independent of the size of the cuttings.

$\bar{l}$ [m]			$\bar{n}_l$ [-]			$\bar{L}_s$ [cm]		
c_3	d_3	R^2	c_4	d_4	R^2	c_5	d_5	R^2
0.02	0.27	0.85	85	-	0.97	55.58	0.63	0.60

329 release of roots from the soil [*Bailey et al.*, 2002; *Mickovski et al.*, 2007] and from root
330 loosening [*Smith*, 2007]. These three different phases are obvious in several of the uproot-
331 ing curves shown in the panels in Figure 6. In previous studies, the maximum root resis-
332 tance exerted by roots was found to increase with total root length [*Bywater-Reyes et al.*,
333 2015; *Ennos*, 1989; *Bailey et al.*, 2002; *Karrenberg et al.*, 2003; *Edmaier et al.*, 2014].
334 The same trend is observed in the present data (Figure 7), where the maximum uproot-
335 ing force, F_{max}, increases linearly with the total root length of the samples, L_r, depending
336 on soil water content [*Pollen*, 2007; *Pollen-Bankhead and Simon*, 2010]. The uprooting
337 force increases also with time, as can be seen by the relationship between the total root
338 length and time depicted in Figure 5a. Moreover, it can be observed that the maximum
339 uprooting force simply depends on the size of the cutting expressed by the total rooting
340 length, which in turn, scales with the cutting size L. This confirms the existence of a pos-
341 sible upscaling law (given the low variability of the cutting diameters). By comparing
342 Figure 7a and 7b, it is also clear how, in fully-saturated conditions (Figure 7a), the max-
343 imum uprooting force is more than about twice lower than the force exerted in unsaturated
344 conditions (Figure 7b). An explanation of this phenomenon is provided by *Wood* [1990]

who argues that undrained stress in saturated soil increases pore-water pressure, causing the frictional strength of the soil to reduce. In turn, this mechanism may enhance the sliding of roots among the sediment particles. To explain why this significant difference in maximum uprooting force occurs under different saturation conditions, we examine the force-displacement curves in Figure 6.

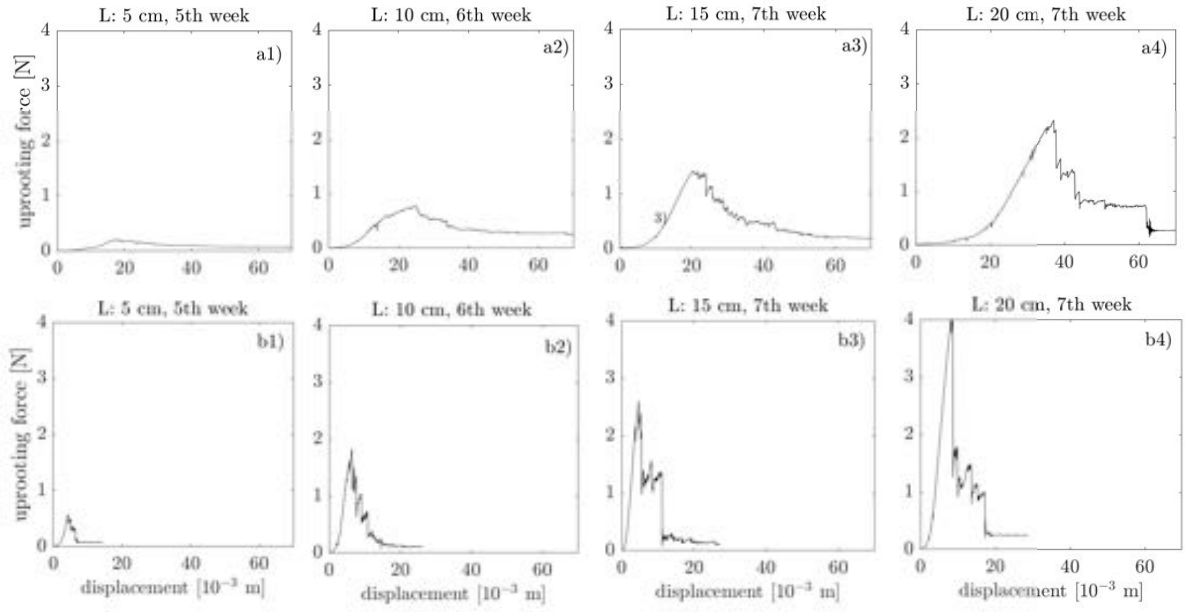

Figure 6. Force-displacement curves for *Salix* cuttings of different size L uprooted at different times. Samples illustrated in panels a) were uprooted under 100% saturation conditions, whereas the others in b) were uprooted under 60% saturation. The panels are arranged in terms of cutting size L and sample uprooting time as follows: a1) L=5 cm and week=5^{th}; a2) L=10 cm, week=6^{th}; a3) L=15 cm, week=7^{th}; a4) L=20 cm, week=7^{th}; b1) L=5 cm and week=5^{th}; b2) L=10 cm, week=6^{th}; b3) L=15 cm, week=7^{th}; b4) L=20 cm, week=7^{th}.

Figure 6 not only shows that the maximum force peak reaches higher values under low saturated conditions, but also illustrates some differences in the descending phase. Typically, in sand of low saturation, the anchoring force decays rapidly, with large and rapid drops following sharp peaks. The trend is more discernible for 20 cm cuttings and less evident as the size of the cuttings diminishes because the load that the plant is required to withstand is smaller. For saturated sand, the descending phase is slower and smoother indicating more uniform friction, with smaller post-peak force oscillations. Similar behaviour was observed by other authors [*Ennos*, 1990; *Schwarz et al.*, 2011; *Edmaier*

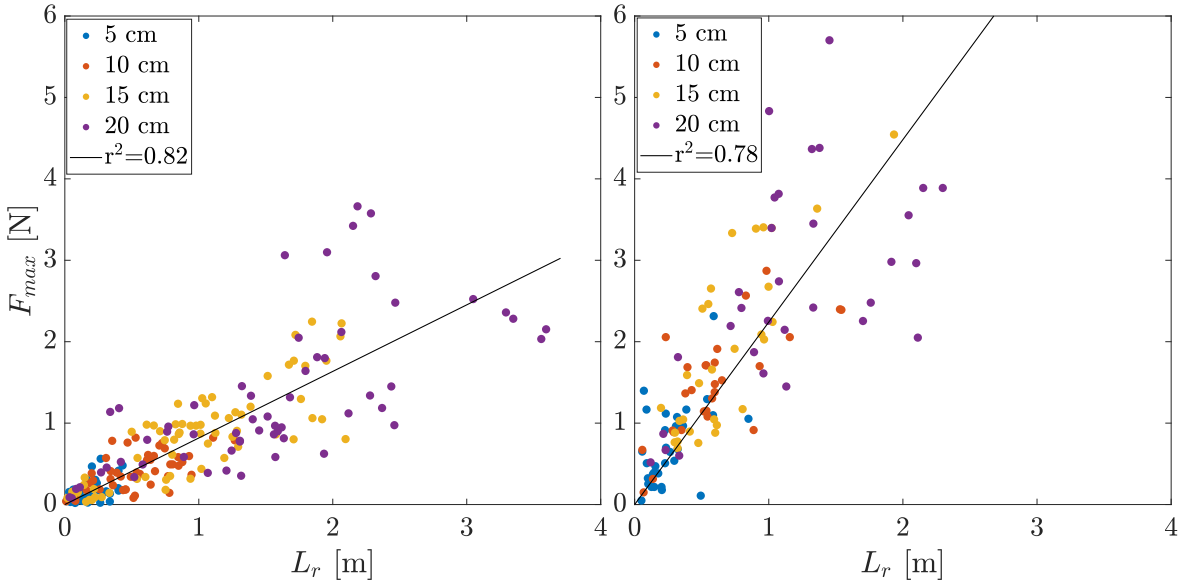

Figure 7. Maximum uprooting force plotted against the total root length. a) 100% saturated medium, with linear fitting law given by F_{max}=0.82·L_r with goodness of fit R^2=0.67 and Pearson coefficient r^2=0.82; b) 60% saturated medium, with linear fitting law given by F_{max}=2.24 ·L_r with goodness of fit R^2=0.54 and Pearson coefficient r^2=0.78.

et al., 2014] and will be further discussed in the following sections. Uprooting work done (Figure 8), evaluated by computing the area under the force-displacement curve, reveals valuable information about the resilience to uprooting of the plant. For 100% sediment moisture content (Figure 8a), the uprooting work done is well approximated by a second degree polynomial law, whereas for a plant uprooted from low saturated sand (Figure 8b) the work done increases linearly with total rooting length albeit with higher variability. These two different trends in uprooting work done may be explained by examining the post-peak phase of the force-displacement curve in Figure 6, where the major portion of the work done is undertaken. By comparing Figure 6a and 6b it can be seen that the uprooting process requires more time in sand that is fully-saturated than under conditions of low-saturation when roots have less resilience because of energy loss occurring over shorter time and space scales.

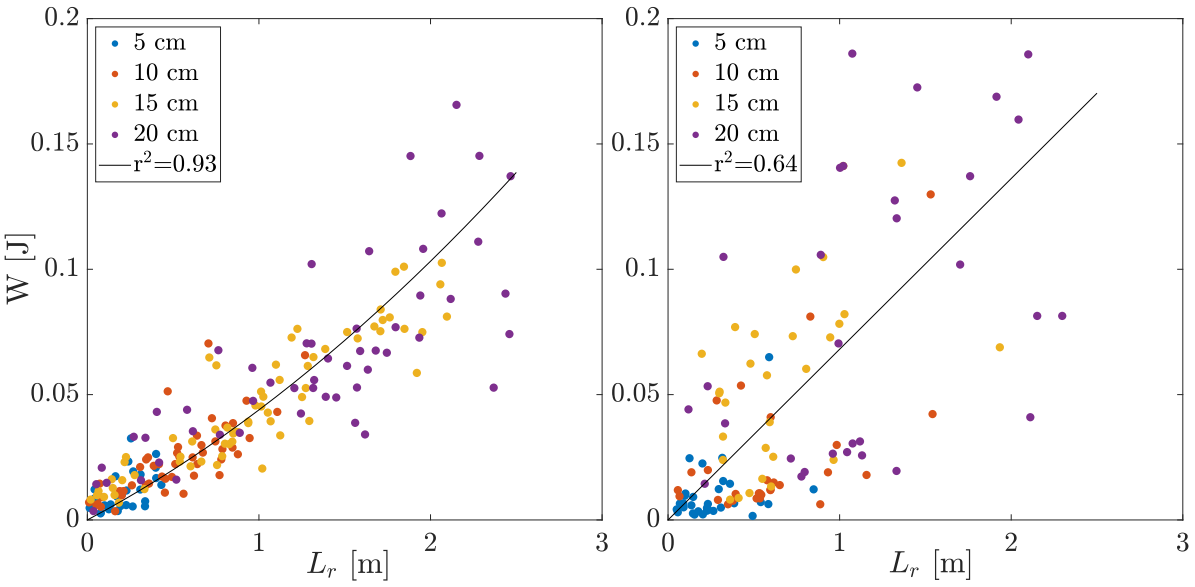

Figure 8. Variation in maximum uprooting work done with total root length: a) 100% saturated medium, where the fitting law is quadratic, W=8·10$^{-7}L_r^2$+4·10$^{-4}L_r$, with goodness of fit R^2=0.83 and correlation coefficient (Spearman coefficient) r^2=0.93; and b) 60% saturated medium, where the fitting law is linear, W=7·10$^{-4}L_r$, with goodness of fit R^2=0.41 and Pearson coefficient r^2=0.64.

3.3 Force drop analysis

Before performing a statistical analysis of force drops, we first define the term 'force drop' and then present a quantitative method for classifying force drops. A force drop corresponds to a monotonic decline in force-time signal between two successive local maximum and minimum values. Given that the monotonic decline has a certain mean gradient, we introduce a parameter that represents the steepness of the force drops and can be used for their classification. The force drop parameter, α, is expressed as the ratio between the local maximum-to-minimum differences between two consecutive force values dF and their respective time-lapses dt (Figure 9a). By varying α, the force drops can be classified according to size and number. Figure 9b shows the variation in ratio of number of force drops in 100% saturated soil, N^F_{100}, to that in 60% saturated soil, N^F_{60}, with α. Values for N^F_{100} and N^F_{60} were obtained by computing the average numbers of force drops determined from force signals for plants uprooted at the same time in saturated and unsaturated conditions. Figure 9b shows that the ratio $\frac{N^F_{100}}{N^F_{60}}$ decreases exponentially for α ≥0.5-0.9 and becomes independent of α when α is close to 1. This leads us to deduce that mild drops oc-

cur more frequently when plants are uprooted from saturated soil. However, the proportion of steep drops is the same regardless of the water sediment content. Figure 10 illustrates the cumulative relative frequencies of force drops magnitude computed for plants of similar root length that are uprooted at the same time under two different sediment moisture conditions, corresponding to Figures 6a4 and 6b4. For $\alpha \geq 0.5$ (Figure 10a), 50% of the force drops of a plant uprooted from saturated sediment have magnitude less than 0.017 N, far below the value of 0.107 N obtained for a plant pulled out from low saturated sediment. For the same value of α, the force drops exhibit a magnitude up to 4 times larger in 100% saturated sediment, than in low saturated sand. A similar trend is observed for $\alpha \geq 1.5$ (Figure 10b). This finding that the magnitude of force drops is higher for less saturated sediment implies stronger adhesion among sediment particles in such cases [*Edmaier et al.*, 2011].

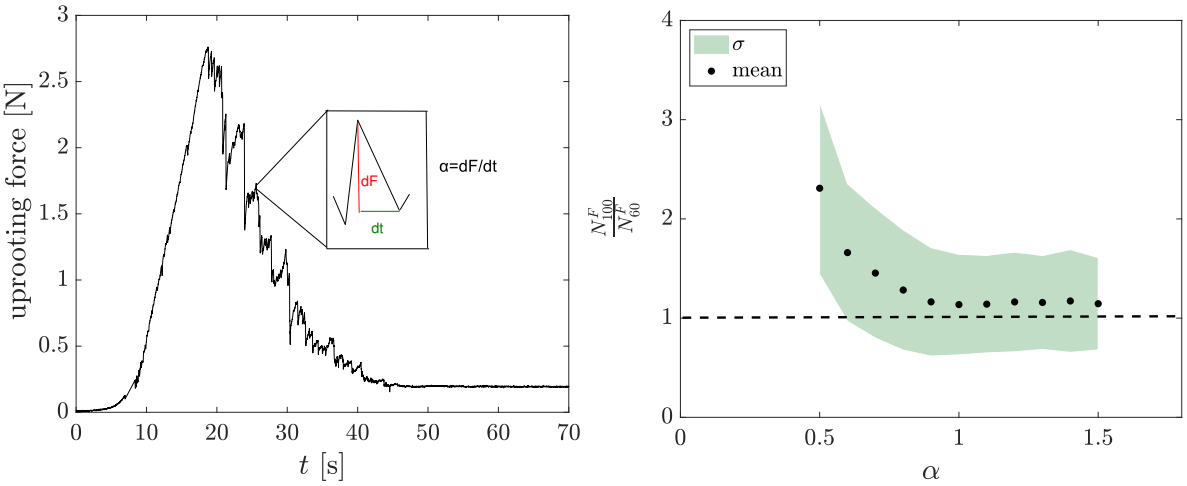

Figure 9. Relationship between uprooting force with time and force drop ratio with α a) generic force-displacement curve illustrating the concepts of dF, dt and α; and b) variation in averaged ratio between the number of force drops in 100% saturated soil to that in 60% saturated soil with α, displaying mean values (dots) and standard deviation σ (green shading).

Therefore, regardless of the magnitude of the force drop sequence, the mechanism controlling downward jumps changes according to the moisture level of the sediment. It is also instructive to compare the autocorrelation function of the dF sequence and the force drops intertime dT sequence. For 100% saturation and $\alpha \geq 0.5$, the autocorrelograms of the force drop and intertime sequences exhibit positive, though low, correlations

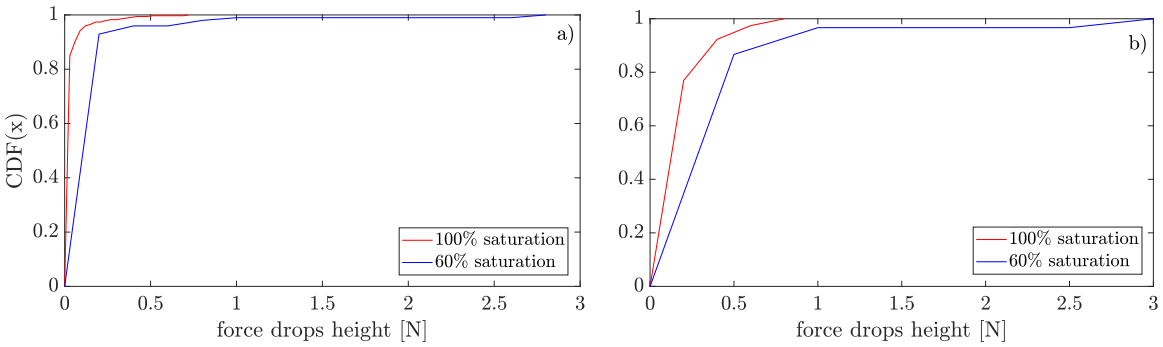

Figure 10. Cumulative relative frequencies of the force drops corresponding to the force-displacement curves in Figure 6a4 (100% saturation) and Figure 6b4 (60% saturation) when: a) $\alpha \geq 0.5$; b) $\alpha \geq 1.5$.

for almost every lag (Figures 11a1 and 11a3). This is most likely due to rearrangement of sand grains in the soil matrix when roots are sliding. In low saturated conditions (Figures 11b1 and 11b3), the correlation is not significant. This discrepancy may be explained as follows: when the medium is entirely saturated, water fills the pores and roots tend to slide between the sand grains. The presence of water modifies the sand grain arrangement around the roots, and causes regular force decay to occur [*Schwarz et al.*, 2011]. Conversely, when the water content in the sediment is lower (60% of water content), the force signal (Figure 6b) presents steeper force drops (steep loosening). Once roots exceed the soil strength, the lower cohesion of sand allows quicker movement of the roots through the grains. Thus, the force drops and their related intertimes assume an autocorrelated 'white' noise structure. Moreover, the large force drops and the related intertimes appear to have a correlation structure with a spatial scale comparable to the smallest fluctuation in the process, i.e. of the order of the sediment grains [*Crouzy et al.*, 2014].

We now analyse the final force recovery event in the force-displacement signal, F_{res}, and compare it to F_{max} (see Figure 12). In the scatter plots in Figure 12, two main regions can be identified. The first region, to the left of the green line, includes mostly small cuttings of which some of the less mature 15-20 cm cuttings have invested all their energy in withstanding the uprooting force. Notably, for fully-saturated soil, the data in the left region are dispersed within a range of $\frac{F_{res}}{F_{max}}$ that is larger than in low-saturated medium. This agrees with the trends in descending phases observed in Figure 6. In 60% saturated soil, the energy loss occurs with large force drops and over shorter time intervals than in 100% saturated soil. This implies that the residual energy of roots may not be

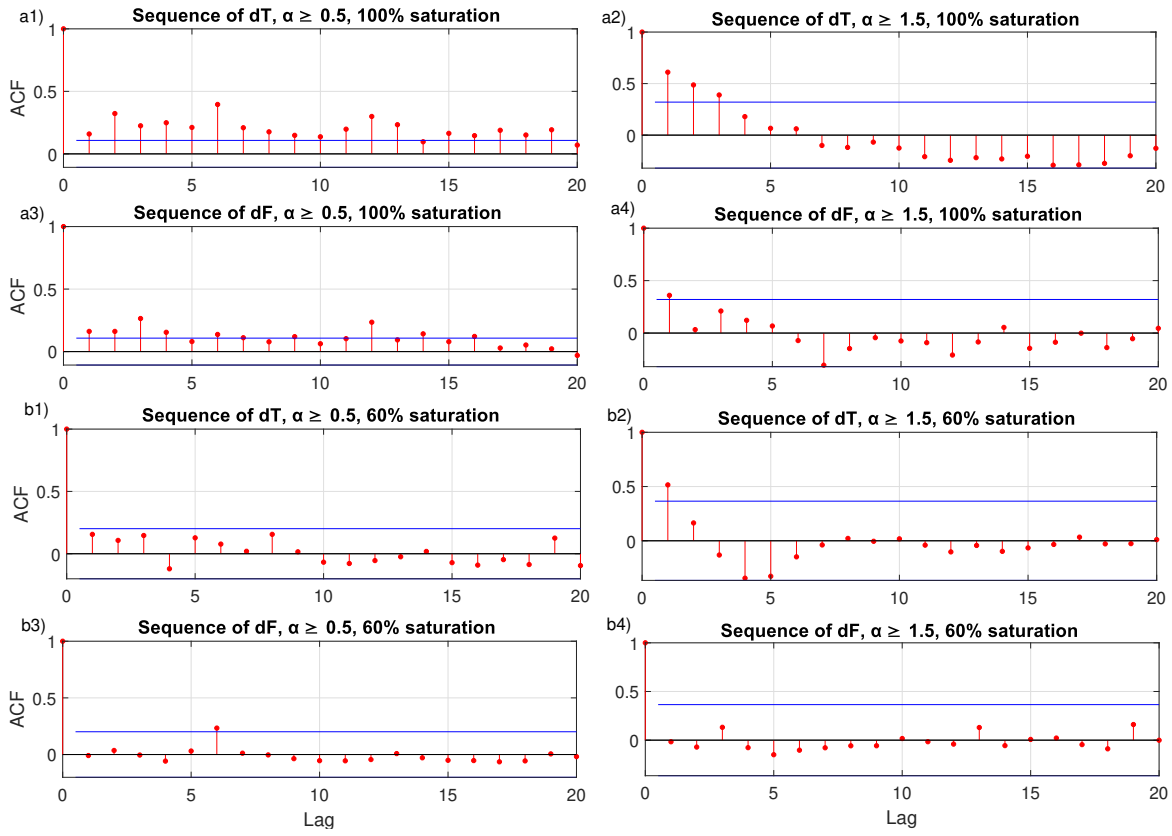

Figure 11. Autocorrelation functions of the force drops dF and their respective intertime dT. The blue solid lines demark confidence bounds. Autocorrelation of the force drops intertime dT for 100% saturation when: a1) $\alpha \geq 0.5$; a2) $\alpha \geq 1.5$; Autocorrelation of the force drops dF for 100% saturation when: a3) $\alpha \geq 0.5$; a4) $\alpha \geq 1.5$. Autocorrelation of the force drops intertime dT for 60% saturation when: b1) $\alpha \geq 0.5$; b2) $\alpha \geq 1.5$; Autocorrelation of the force drops dF for 60% saturation when: b3) $\alpha \geq 0.5$; b4) $\alpha \geq 1.5$.

sufficient to generate a resistance F_{res} comparable to F_{max}. Region II includes cuttings uprooted at a later stage of growth, when $\frac{F_{res}}{F_{max}}$ is almost constant regardless of the value of F_{max}. The presence of mature plants in the right hand region indicates that older plants can have higher resilience. A similar division of $\frac{F_{res}}{F_{max}}$ data into two regions with respect to F_{max} was also observed by *Crouzy et al.* [2014] for *Avena sativa* plants.

4 Uprooting by flow

Plant uprooting by flow occurs whenever the action of the drag and the net buoyancy forces equal the root resistance exerted by total root length of the plant $\mathbf{R}(L_r)$ [*Ed-*

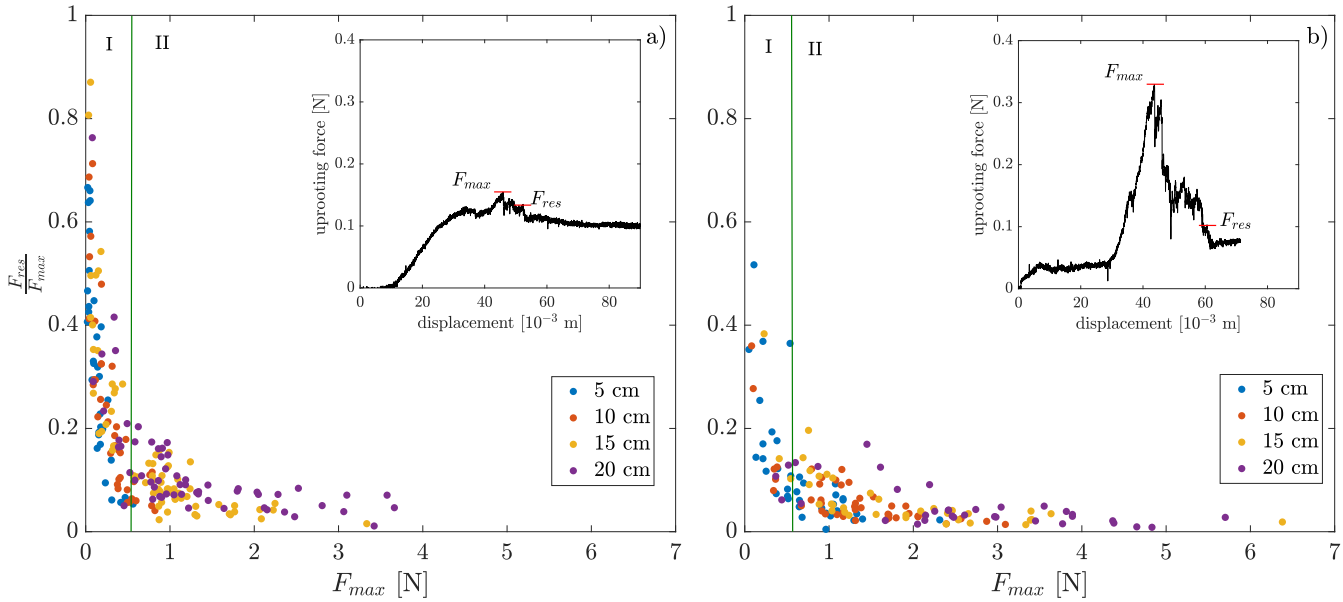

Figure 12. $\frac{F_{res}}{F_{max}}$ versus F_{max} for uprooting in: a) 100% saturation soil; b) 60% saturated soil. The inset panels comprise force-displacement curves on which are marked the maximum uprooting force F_{max} and the residual force F_{res} at which failure of the last plant fiber occurs.

maier et al., 2014]. The force may be expressed as:

$$\mathbf{F_{d,n}} + \mathbf{F_{d,t}} + \mathbf{F_n} = \mathbf{R}(L_r), \tag{5}$$

where $\mathbf{F_{d,n}}$ is the normal component of the drag force, $\mathbf{F_{d,t}}$ is the tangential component of the drag force, and $\mathbf{F_n}$ is the net buoyancy force. When the root resistance $\mathbf{R}(L_r)$ equals the pulling force $\mathbf{F}_{max}$ for an equal root length in static conditions, equation (5) reads:

$$\mathbf{F_{d,n}} + \mathbf{F_{d,t}} + \mathbf{F_n} = \mathbf{F_{max}}(L_r), \tag{6}$$

where $\mathbf{F_{max}}(L_r)$ relates to the fitting law extrapolated under saturated conditions (Figure 7a), such that:

$$F_{max} = 0.82 \cdot L_r \tag{7}$$

Herein, the net buoyancy force $\mathbf{F_n}$ is neglected, following previous studies [*Bywater-Reyes et al.*, 2015; *Calvani et al.*, 2019; *Bau et al.*, 2019]. From a graphical perspective, uprooting takes place when the drag surpasses the root maximum resistance curve. In order to be able to plot the drag force and the resistance law, the drag force is expressed as a function of the total root length L_r. Hence, it is necessary to express both the total surface

area of the stem A_s and the total projected area of the leaves A_l, which appear in the modulus of $\mathbf{F_{d,t}}$ (equation 3), in terms of L_r. The total surface area of the stem is given by:

$$A_s = \pi d_s \left(\frac{\bar{L}_{s,max}}{1 + e^{[-b((\frac{\bar{L}_r}{c_1})^{\frac{1}{d_1}} - t_0)]}} \right) \tag{8}$$

where d_s is the diameter of the cylinder, and the expression in parenthesis is the logistic curve (equation 4) rewritten in terms of $\bar{L}_r$ by invoking the link between time and the averaged root length extrapolated from Figure 5a. The projected area of the leaves is given by:

$$A_l = \frac{d_L d_l}{2} \left[c_4 \left(\frac{\bar{L}_{s,max}}{1 + e^{[-b((\frac{L_r}{c_1})^{\frac{1}{d_1}} - t_0)]}} \right) \right] \tag{9}$$

where d_L and d_l are the length of the two diagonals of the rhombus and the term in square brackets is obtained using the correlation law between the number of leaves and the stem length extrapolated from Figure 5e. The projected area A_n of the trunk that appears in the expression of the normal component of the drag force (equation 2) depends linearly on the size of the cutting L:

$$A_n = \frac{L\bar{d}}{2} \tag{10}$$

Under the reasonable assumption that $\bar{L}_r \approx L_r$, the modulus of the drag force can be expressed as follows:

$$F_d = \frac{1}{2}\rho C_d u^2 \frac{L\bar{d}}{2} + \frac{1}{2}\rho C_f u^2 \left[\pi d_s \left(\frac{\bar{L}_{s,max}}{1 + e^{[-b((\frac{L_r}{c_1})^{\frac{1}{d_1}} - t_0)]}} \right) + \frac{d_L d_l}{2} c_4 \left(\frac{\bar{L}_{s,max}}{1 + e^{[-b((\frac{L_r}{c_1})^{\frac{1}{d_1}} - t_0)]}} \right) \right] \tag{11}$$

Figure 13a displays the trends in dimensionless drag force, $\hat{F}_d$, and maximum root resistance, $\hat{R}(L_r)$, with increasing L_r. The plot refers to a cutting with L=20 cm and a fixed value of u. The dimensionless forms were obtained by dividing equations 7 and 11, respectively, by the product: $\rho \frac{1}{2} C_f u^2 \bar{d}^2$, such that the drag force is parametrized by L, whereas the root resistance scales with u. It is obvious that uprooting occurs within two temporal windows. The first one, I, is located at the very early stage of plant growth when the root length is still small and the curve of the drag forces is convex. The second window, II, occurs in the section of the curve that coincides with the terminal growth stage of the plants. The occurrence of biological time windows is reminiscent of a concept introduced by *Balke et al.* [2011], who studied the threshold for the establishment of mangrove seedling on tidal flats. Figure 13b shows the trend in dimensionless drag force with root length L_r for all values of cutting length L. Here, $\hat{R}(L_r)$ is plotted for increasing values

of u (grey lines). The $\hat{F}_d$ curves cross the L_r=0 axis at different ordinate values. This is because when wood logs have not yet developed any above- and below- ground biomass, the drag force acts only on the portion of the trunk exposed to the flow. Over a certain range of low flow velocities, wood logs can provide resistance to drag forces without any contribution from root resistance. Importantly, this means that the present model is applicable both to species able to reproduce asexually, and to species incapable of resprouting. Figure 13b also shows that drag force curves interrupt at values of L_r that increase progressively with L. Unlike the root resistance curve, the trend in drag force is therefore affected by the size of the cuttings.

5 Discussion

Although previous studies documented the importance of studying wood regime dynamics in river basins, a full understanding was not developed as to how the biomechanical properties of regenerated living wood impact its remobilization. In the present study, we examine the anchoring resistance and the growth performance of small-scale logs of *Salix fragilis*, a species that colonizes wide areas along rivers and spreads through vegetative reproduction. Our results confirm that knowledge of the time histories of regrowth of stranded wood fragments and associated root resistance is fundamentally important in the analysis of wood dynamics in rivers. In fact, the statistics of plant growth and force-displacement parameters are valuable tools for quantitative study of the variation in drag forces and deterministic prediction of the growth stages of logs when remobilization may occur. Herein, the evolution of plant biomass was presented in terms of sample averages, and extrapolated growth laws then fitted to parameters representing below- and above-ground biomass. In general, the growth trends exhibit power-law behaviour in terms of root length, number of roots, and average root depth. Due to a lack of studies where destructive measurements have been taken, it is hard to deduce whether power fitting curves can be used to describe the average growth trends of other species and under different water table conditions. However, for example, based on the experiments of *Imada et al.* [2008], it has been found that power trends can approximate well the evolution of the root length of samples of *Populus alba* tested under different water table conditions. It should be noted that over the duration of the present experiments, root growth tended to be confined, on average, within the unsaturated zone, about 6 cm deep. Given that this depth depends primarily on soil texture, we expect it to be an important factor regarding the extent

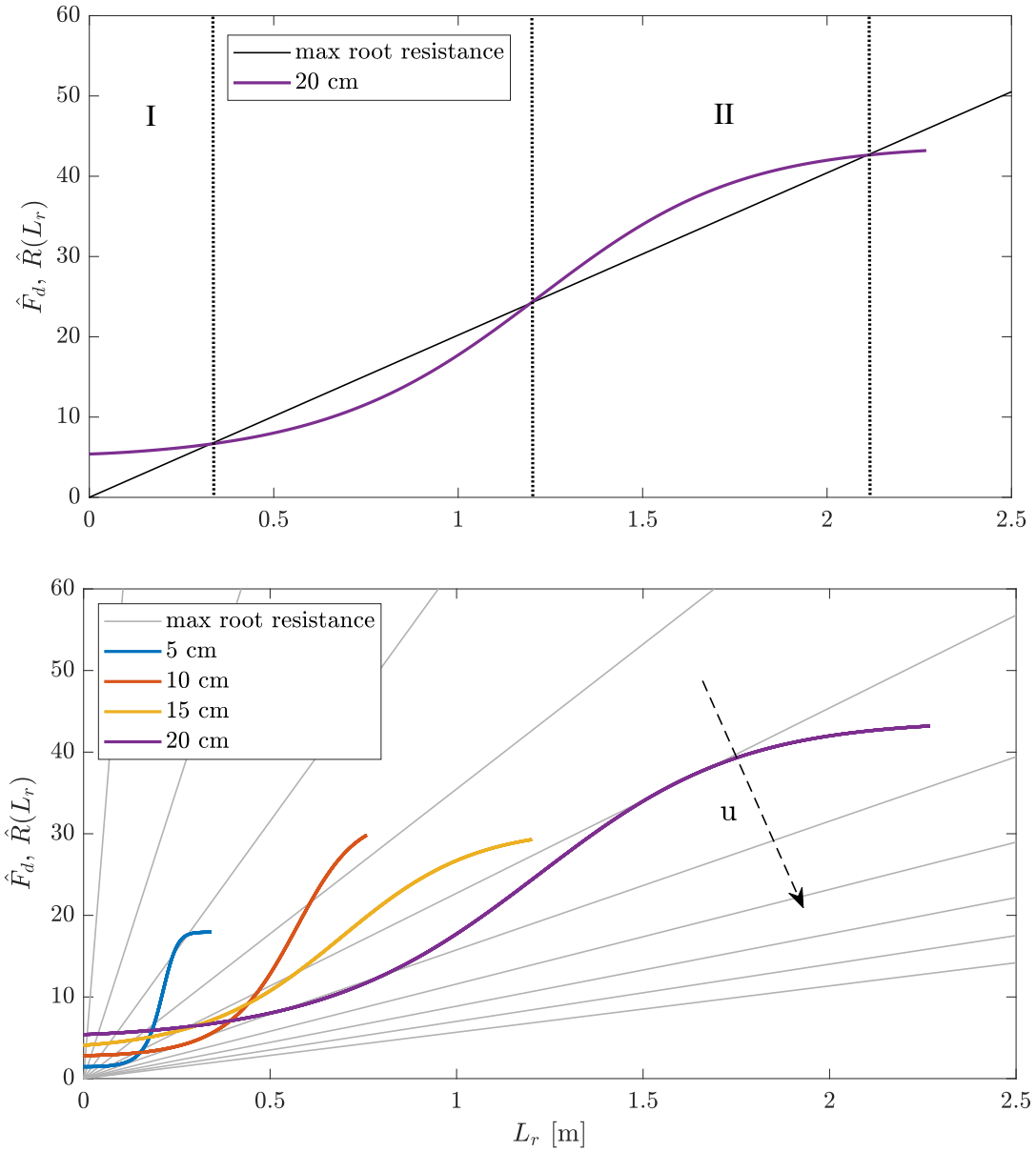

Figure 13. Representation of variations in dimensionless drag force and maximum root resistance with root length: a) cutting size L=20 cm and fixed flow velocity u; and b) all cutting sizes L and different values of u.

and growth rate of below-ground biomass. The results have demonstrated that the average trends in vegetation growth characteristics are statistically significant. We now consider data variability. Low goodness of fit values were obtained from the below-ground biomass trends for cuttings of 5 cm length (see Table 2). The variability is due to the intrinsic randomness of plant development and to heterogeneity of plant characteristics. Even though cuttings were collected from the same tree, some did not develop roots, some died, and

some sprouted quicker than others even if subjected to the same external conditions (e.g. sediment, water percentage availability, and stable environment temperature). The variability in the data may also be attributed to the limited number of samples when computing statistical averages. Concerning the above-ground biomass, the logistic law was found to approximate well the growth trends of the cuttings, until all their nutrient resources had been depleted. Analysis of the force drops in the force-displacement curves enabled us to identify statistically the way in which force exerted by and energy stored in the roots are released under different soil moisture conditions. The present analysis has helped elucidate several important features of the uprooting mechanisms that to our knowledge had remained unexplored to date. In addition, the trend in root surface area along the cuttings and the link between uprooting force and total root length have revealed promising information in terms of upscaling.

Several limitations should be considered. First, even though *Salix fragilis* is one of Europe's largest native willows, the growth characteristics of this species may not be representative of all species belonging to *Salicaceae* family. Hence, further investigations are needed to assess other species characteristics. A second limitation is that the scouring processes, accounted in the free-body model of *Bau et al.* [2019], were not considered here. As a consequence, the type of uprooting simulated here is of Type I. This simplification is nevertheless consistent with the young growth state of the samples considered. However, our data interpretation is not yet applicable to more mature vegetation, for which the scouring around the plant would need to be taken into account, and for which the sedimentary structure and bed morphology around the plant will have evolved. At field scale and for more mature vegetation, the influence of sediment calibre and the evolution of the riverbed around the deposited wood (e.g. due to scour processes or fine sediment trapping) still need to be properly tackled. In a more complex scenario, stochastic sources that are not considered herein (e.g. river processes, the effect of turbulence and flapping mechanism) should also be taken into account, given their cumulative contribution to the uprooting process [*Perona and Crouzy*, 2018]. Another aspect to consider is the assumption concerning the impact angle of flow-cutting. When computing the drag force, the cases solely considered flow impact perpendicular to the longitudinal cross section of the log. Impacts at other angles were not examined, but warrant future investigation. A further limitation of the present work is the formulation of the stem length as a total quantity without considering the number of branches. Such conditions lead to underestimation of

570 the tangential component of the drag force acting on the surface area of vegetation. An-
571 other constraint arises from having expressed the maximum uprooting force as a function
572 of total rooting length, which implies that the strength exerted by a long root results from
573 the summed individual root strength, assuming perfect cooperation among roots [*Ennos*,
574 1993]. However, it is quite possible that the pullout force is not built up by individual and
575 simultaneous contributions of all the roots [*Pollen and Simon*, 2005; *Schwarz et al.*, 2011;
576 *Pollen-Bankhead and Simon*, 2009]. In fact, roots are not pulled in parallel; instead up-
577 rooting is a slightly cumulative process, as described by *Edmaier* [2014], whereby a given
578 root becomes strained just after the loosening of another root previously under tension.
579 It should nevertheless be noted that the calculation of maximum root resistance included
580 contributions provided by root hairs and secondary roots, whose cooperation is significant
581 in multi-root systems [*Bailey et al.*, 2002; *Ennos*, 1989].

582 ## 6 Conclusions

583 Vertical pull-out experiments were carried out at the early-stage of growth, in the
584 context of wood log uprooting, survival, and re-mobilization in rivers during intermit-
585 tent moderate flooding events. Tests were carried out on root reaction to a vertical pulling
586 force for plants in soil with different water availability. Sample cuttings of four different
587 lengths but nearly constant diameter were considered, the aim being to develop upscaling
588 rules. Force drops in the force-displacement signal were examined to assess how a change
589 in soil moisture percentage can influence the uprooting process. Fitting laws extrapolated
590 from the plant growth statistics facilitated computation of an analytical expression of the
591 drag force and enables definition of the threshold at which a wood log, at a certain stage
592 of growth, becomes sufficiently resilient to withstand a given hydrologic event. By equat-
593 ing the flow-induced drag force to maximum root resistance, an expression was derived for
594 root lengths contributing to the resistant force and, more importantly, time windows when
595 uprooting may occur. It was found that a certain threshold value of impact flow velocity
596 had to be reached in order to obtain two distinct uprooting windows. From the analysis,
597 it was deduced that the modulus of drag force and (accordingly) the flow velocity have to
598 increase progressively when removing a cutting of increasing size. Despite several limi-
599 tations (see Discussion), the present analysis provides a useful means by which to inform
600 new flood protection measures and to understand the contribution of wood logs to river
601 ecology, management, and restoration. It is hoped that the present experiments will be

602 further reproduced (e.g. for different diameters of cuttings) in order to develop upscaling
603 rules that would facilitate the derivation of useful allometric laws. The data collected and
604 analysed as part of the present investigation are freely available to interested parties, the
605 intention being to support the development of more efficient wood dynamics models that
606 incorporate biomechanical properties of representative plant species.

607 **A: Nomenclature**

Table A.1: Nomenclature Used in the Paper.

Symbol	Description	Unit
A_l	total surface area of the foliage	[L^2]
A_n	drag exposed projected area of the trunk	[L^2]
A_s	total surface area of the stems	[L^2]
b	logistic growth rate	[T^{-1}]
C_D	drag coefficient	[-]
C_f	friction coefficient	[-]
$\bar{d}$	averaged diameter of the wood log	[L]
dF	force drop height	[M· L· T^{-2}]
d_L	major diagonal of the rhombus	[L]
d_l	minor diagonal of the rhombus	[L]
dt	force drop duration	[T]
dT	force drops intertime	[T]
$F_{d,n}$	drag force	[M· L· T^{-2}]
$F_{d,t}$	friction force	[M· L· T^{-2}]
$\hat{F}_d$	dimensionless drag force	[-]
F_n	net buoyancy force	[M· L· T^{-2}]
F_{res}	last force recovery	[M· L· T^{-2}]
F_{max}	maximum uprooting force	[M· L· T^{-2}]
L	cutting length	[L]
L_r	total root length	[L]
$\bar{L}_r$	average total root length	[L]
$\bar{L}_s$	average total stem length	[L]
$\bar{L}_{s,max}$	averaged total stem length at the maximum growth stage	[L]
$\bar{l}$	average root depth	[L]
N_{100}^F	number of force drops in 100% saturation	[-]
N_{60}^F	number of force drops in 60% saturation	[-]
$\bar{n}_l$	averaged number of leaves	[-]
$\bar{n}_r$	averaged number of roots	[-]
R	maximum root resistance	[M· L· T^{-2}]

Continued on next page

Table A.1 – continued from previous page

Symbol	Description	Unit
$\hat{R}$	dimensionless maximum root resistance	[-]
t	time	[T]
t_0	location of the sigmoid's midpoint	[T]
u	flow velocity impacting the log	[L· T^{-1}]
$\bar{V}_r$	averaged root volume	[L^3]
W	uprooting work	[M· L^2· T^{-2}]
$\tilde{x}$	normalised values of the cutting lengths	[-]
α	ratio between dF and dt	[M· L· T^{-3}]
ρ_w	water density	[M· L^{-3}]
σ	standard deviation	[-]
ω	root surface area per unit length	[L^2]

Acknowledgments

We want to express our extreme gratitude to Prof Alistair Borthwick for his assistance in revising and editing this manuscript. Acknowledgments are also extended to Danny-Lee Greiner and Rahul Bharadwaj Prakash for their assistance in carrying out the experiments. We do not report any conflicts of interest. The dataset used in this manuscript can be found online on Zenodo (http://doi.org/10.5281/zenodo.3985848).

References

Abbe, T. B., and D. R. Montgomery (1996), Large woody debris jams, channel hydraulics and habitat formation in large rivers, *Regulated Rivers: research & management*, *12*(2-3), 201–221.

Anderson, N. H., J. R. Sedell, L. M. Roberts, and F. J. Triska (1978), The role of aquatic invertebrates in processing of wood debris in coniferous forest streams, *American Midland Naturalist*, pp. 64–82.

Bailey, P. H., J. Currey, and A. Fitter (2002), The role of root system architecture and root hairs in promoting anchorage against uprooting forces in allium cepa and root mutants

of arabidopsis thaliana, *Journal of Experimental Botany*, *53*(367), 333–340.

Balke, T., T. J. Bouma, E. M. Horstman, E. L. Webb, P. L. Erftemeijer, and P. M. Herman (2011), Windows of opportunity: thresholds to mangrove seedling establishment on tidal flats, *Marine Ecology Progress Series*, *440*, 1–9.

Bankhead, N. L., R. E. Thomas, and A. Simon (2017), A combined field, laboratory and numerical study of the forces applied to, and the potential for removal of, bar top vegetation in a braided river, *Earth Surface Processes and Landforms*, *42*(3), 439–459.

Bau, V., S. Zen, G. Calvani, and P. Perona (2019), Extracting the critical rooting length in plant uprooting by flow from pullout experiments, *Water Resources Research*.

Bebi, P., D. Kulakowski, and C. Rixen (2009), Snow avalanche disturbances in forest ecosystems—state of research and implications for management, *Forest ecology and Management*, *257*(9), 1883–1892.

Beckman, N. D., and E. Wohl (2014), Carbon storage in mountainous headwater streams: The role of old-growth forest and logjams, *Water Resources Research*, *50*(3), 2376–2393.

Benda, L., D. Miller, J. Sias, D. Martin, R. Bilby, C. Veldhuisen, and T. Dunne (2003), Wood recruitment processes and wood budgeting, in *American Fisheries Society Symposium*, pp. 49–74, American Fisheries Society.

Bendix, J., and C. R. Hupp (2000), Hydrological and geomorphological impacts on riparian plant communities, *Hydrological processes*, *14*(16-17), 2977–2990.

Bocchiola, D., F. Catalano, G. Menduni, and G. Passoni (2002), An analytical–numerical approach to the hydraulics of floating debris in river channels, *Journal of Hydrology*, *269*(1-2), 65–78.

Braudrick, C. A., and G. E. Grant (2000), When do logs move in rivers?, *Water resources research*, *36*(2), 571–583.

Braudrick, C. A., G. E. Grant, Y. Ishikawa, and H. Ikeda (1997), Dynamics of wood transport in streams: a flume experiment, *Earth Surface Processes and Landforms: The Journal of the British Geomorphological Group*, *22*(7), 669–683.

Brooks, A. P., and G. J. Brierley (2002), Mediated equilibrium: the influence of riparian vegetation and wood on the long-term evolution and behaviour of a near-pristine river, *Earth Surface Processes and Landforms: The Journal of the British Geomorphological Research Group*, *27*(4), 343–367.

Bywater-Reyes, S., A. C. Wilcox, J. C. Stella, and A. F. Lightbody (2015), Flow and scour constraints on uprooting of pioneer woody seedlings, *Water Resources Research*, *51*(11), 9190–9206.

Cadol, D., E. Wohl, J. R. Goode, and K. L. Jaeger (2009), Wood distribution in neotropical forested headwater streams of la selva, costa rica, *Earth Surface Processes and Landforms*, *34*(9), 1198–1215.

Calvani, G., S. Francalanci, and L. Solari (2019), A physical model for the uprooting of flexible vegetation on river bars, *Journal of Geophysical Research: Earth Surface*, *124*(4), 1018–1034.

Comiti, F., A. Lucía, and D. Rickenmann (2016), Large wood recruitment and transport during large floods: a review, *Geomorphology*, *269*, 23–39.

Corenblit, D., A. C. Baas, G. Bornette, J. Darrozes, S. Delmotte, R. A. Francis, A. Gurnell, F. Julien, R. J. Naiman, and J. Steiger (2011), Feedbacks between geomorphology and biota controlling earth surface processes and landforms: a review of foundation concepts and current understandings, *Earth-Science Reviews*, *106*(3-4), 307–331.

Coutts, M. (1983), Root architecture and tree stability, in *Tree root systems and their mycorrhizas*, pp. 171–188, Springer.

Crouzy, B., K. Edmaier, and P. Perona (2014), Biomechanics of plant anchorage at early development stage, *Journal of theoretical biology*, *363*, 22–29.

Daniels, M. D. (2006), Distribution and dynamics of large woody debris and organic matter in a low-energy meandering stream, *Geomorphology*, *77*(3-4), 286–298.

Décamps, H., and R. J. Naiman (1990), *The ecology and management of aquatic-terrestrial ecotones*, vol. 4, CRC Press.

Downs, P. W., and A. Simon (2001), Fluvial geomorphological analysis of the recruitment of large woody debris in the yalobusha river network, central mississippi, usa, *Geomorphology*, *37*(1-2), 65–91.

Edmaier, K., P. Burlando, and P. Perona (2011), Mechanisms of vegetation uprooting by flow in alluvial non-cohesive sediment, *Hydrology and Earth System Sciences*, *15*(5), 1615–1627.

Edmaier, K., B. Crouzy, R. Ennos, P. Burlando, and P. Perona (2014), Influence of root characteristics and soil variables on the uprooting mechanics of avena sativa and medicago sativa seedlings, *Earth Surface Processes and Landforms*, *39*(10), 1354–1364.

Edmaier, K. M. (2014), Uprooting mechanisms of juvenile vegetation by flow erosion, *Tech. rep.*, EPFL.

Ennos, A. (1993), The scaling of root anchorage, *Journal of Theoretical Biology*, *161*(1), 61 – 75, doi:https://doi.org/10.1006/jtbi.1993.1040.

Ennos, A., and S. Pellerin (2000), *Root methods: A handbook*, chap. Plant Anchorage, pp. 545–565, Springer.

Ennos, A. R. (1989), The mechanics of anchorage in seedlings of sunflower, helianthus annuus l., *New Phytologist*, *113*(2), 185–192.

Ennos, A. R. (1990), The anchorage of leek seedlings: the effect of root length and soil strength, *Annals of Botany*, *65*(4), 409–416.

Fisher, S. G., and G. E. Likens (1972), Stream ecosystem: organic energy budget, *BioScience*, *22*(1), 33–35.

Francis, R. A. (2007), Size and position matter: riparian plant establishment from fluvially deposited trees, *Earth Surface Processes and Landforms*, *32*(8), 1239–1243.

Francis, R. A., and A. M. Gurnell (2006), Initial establishment of vegetative fragments within the active zone of a braided gravel-bed river (river tagliamento, ne italy), *Wetlands*, *26*(3), 641–648.

Francis, R. A., A. M. Gurnell, G. E. Petts, and P. J. Edwards (2005), Survival and growth responses of populus nigra, salix elaeagnos and alnus incana cuttings to varying levels of hydric stress, *Forest Ecology and Management*, *210*(1-3), 291–301.

Francis, R. A., P. Tibaldeschi, and L. McDougall (2008), Fluvially-deposited large wood and riparian plant diversity, *Wetlands Ecology and Management*, *16*(5), 371–382.

Gasser, E., M. Schwarz, A. Simon, P. Perona, C. Phillips, J. Hübl, and L. Dorren (2019), A review of modeling the effects of vegetation on large wood recruitment processes in mountain catchments, *Earth-Science Reviews*.

Gippel, C. J., I. C. O'NEILL, B. L. FINLAYSON, and I. Schnatz (1996), Hydraulic guidelines for the re-introduction and management of large woody debris in lowland rivers, *Regulated Rivers: Research & Management*, *12*(2-3), 223–236.

Gregory, S. V., F. J. Swanson, W. A. McKee, and K. W. Cummins (1991), An ecosystem perspective of riparian zones, *BioScience*, *41*(8), 540–551.

Gregory, S. V., M. A. Meleason, and D. J. Sobota (2003), Modeling the dynamics of wood in streams and rivers, in *American Fisheries Society Symposium*, vol. 37, pp. 315–335, Citeseer.

721 Grunell, A. (1997), The hydrological and geomorphological significance of forested flood-
722 plains, *Global Ecology and Biogeography Letters*, pp. 219–229.

723 Guilloy, H., E. González, E. Muller, F. M. Hughes, and N. Barsoum (2011), Abrupt drops
724 in water table level influence the development of populus nigra and salix alba seedlings
725 of different ages, *Wetlands*, *31*(6), 1249–1261.

726 Gurnell, K. Gregory, and G. E. Petts (1995), The role of coarse woody debris in forest
727 aquatic habitats: implications for management, *Aquatic conservation: marine and fresh-*
728 *water ecosystems*, *5*(2), 143–166.

729 Gurnell, A., and G. Petts (2006), Trees as riparian engineers: the tagliamento river, italy,
730 *Earth Surface Processes and Landforms: The Journal of the British Geomorphological*
731 *Research Group*, *31*(12), 1558–1574.

732 Gurnell, A., P. J. Edwards, G. E. Petts, and J. V. Ward (2000), A conceptual model for
733 alpine proglacial river channel evolution under changing climatic conditions, *Catena*,
734 *38*(3), 223–242.

735 Gurnell, A., H. Piégay, F. Swanson, and S. Gregory (2002), Large wood and fluvial pro-
736 cesses, *Freshwater Biology*, *47*(4), 601–619.

737 Gurnell, A., K. Tockner, P. Edwards, and G. Petts (2005), Effects of deposited wood on
738 biocomplexity of river corridors, *Frontiers in Ecology and the Environment*, *3*(7), 377–
739 382.

740 Gurnell, A. M., and G. E. Petts (2002), Island-dominated landscapes of large floodplain
741 rivers, a european perspective, *Freshwater Biology*, *47*(4), 581–600.

742 Gurnell, A. M., G. E. Petts, D. M. Hannah, B. P. G. Smith, P. J. Edwards, J. Kollmann,
743 J. V. Ward, and K. Tockner (2001), Riparian vegetation and island formation along the
744 gravel-bed fiume tagliamento, italy, *Earth Surface Processes and Landforms*, *26*(1), 31–
745 62.

746 Gurnell, A. M., W. Bertoldi, and D. Corenblit (2012), Changing river channels: The roles
747 of hydrological processes, plants and pioneer fluvial landforms in humid temperate,
748 mixed load, gravel bed rivers, *Earth-Science Reviews*, *111*(1-2), 129–141.

749 Howell, J., D. Benson, and L. McDougall (1994), Developing a strategy for rehabilitating
750 riparian vegetation of the hawkesbury-nepean river, sydney, australia, *Pacific Conserva-*
751 *tion Biology*, *1*(3), 257–271.

752 Hsu, F., C. Nelson, and W. Chow (1984), A mathematical model to utilize the logistic
753 function in germination and seedling growth, *Journal of Experimental Botany*, *35*(11),

1629–1640.

Hughes, F. M., T. Harris, K. Richards, G. Pautou, A. El Hames, N. Barsoum, J. Girel, J.-L. Peiry, and R. Foussadier (1997), Woody riparian species response to different soil moisture conditions: laboratory experiments on alnus incana (l.) moench, *Global Ecology and Biogeography Letters*, pp. 247–256.

Hungr, O., S. Evans, and I. Hutchinson (2001), A review of the classification of landslides of the flow type, *Environmental & Engineering Geoscience*, *7*(3), 221–238.

Imada, S., N. Yamanaka, and S. Tamai (2008), Water table depth affects populus alba fine root growth and whole plant biomass, *Functional Ecology*, *22*(6), 1018–1026.

Iroumé, A., L. Mao, A. Andreoli, H. Ulloa, and M. P. Ardiles (2015), Large wood mobility processes in low-order chilean river channels, *Geomorphology*, *228*, 681–693.

Järvelä, J. (2002), *Determination of flow resistance of vegetated channel banks and floodplains*, pp. 311–318, Swets & Zeitlinger, Lisse.

Johnston, C. A., and R. J. Naiman (1987), Boundary dynamics at the aquatic-terrestrial interface: the influence of beaver and geomorphology, *Landscape Ecology*, *1*(1), 47–57.

Karrenberg, S., P. J. Edwards, and J. Kollmann (2002), The life history of salicaceae living in the active zone of floodplains, *Freshwater Biology*, *47*(4), 733–748.

Karrenberg, S., S. Blaser, J. Kollmann, T. Speck, and P. Edwards (2003), Root anchorage of saplings and cuttings of woody pioneer species in a riparian environment, *Functional ecology*, *17*(2), 170–177.

Keller, E. A., and F. J. Swanson (1979), Effects of large organic material on channel form and fluvial processes, *Earth surface processes*, *4*(4), 361–380.

Lassettre, N. S., H. Piégay, S. Dufour, and A.-J. Rollet (2008), Decadal changes in distribution and frequency of wood in a free meandering river, the ain river, france, *Earth Surface Processes and Landforms: The Journal of the British Geomorphological Research Group*, *33*(7), 1098–1112.

Latterell, J. J., J. Scott Bechtold, T. C. O'KEEFE, R. Van Pelt, and R. J. Naiman (2006), Dynamic patch mosaics and channel movement in an unconfined river valley of the olympic mountains, *Freshwater Biology*, *51*(3), 523–544.

Likens, G. E., and F. H. Bormann (1974), Linkages between Terrestrial and Aquatic Ecosystems, *BioScience*, *24*(8), 447–456, doi:10.2307/1296852.

MacVicar, B., and H. Piégay (2012), Implementation and validation of video monitoring for wood budgeting in a wandering piedmont river, the ain river (france), *Earth Surface*

Processes and Landforms, *37*(12), 1272–1289.

Malanson, G. P. (1993), *Riparian landscapes*, Cambridge University Press.

Mao, L., A. Andreoli, A. Iroumé, F. Comiti, and M. A. Lenzi (2013), Dynamics and management alternatives of in-channel large wood in mountain basins of the southern andes, *Bosque*, *34*(3), 319–330.

Martin, D. J., and L. E. Benda (2001), Patterns of instream wood recruitment and transport at the watershed scale, *Transactions of the American Fisheries Society*, *130*(5), 940–958.

Mickovski, S., A. Bengough, M. Bransby, M. Davies, P. Hallett, and R. Sonnenberg (2007), Material stiffness, branching pattern and soil matric potential affect the pullout resistance of model root systems, *European Journal of soil science*, *58*(6), 1471–1481.

Moggridge, H. L. (2007), The dispersal establishment and growth of vegetation in riparian environments, Ph.D. thesis, King's College London (University of London).

Montgomery, D. R., B. D. Collins, J. M. Buffington, and T. B. Abbe (2003), Geomorphic effects of wood in rivers, in *American Fisheries Society Symposium*, vol. 37, pp. 21–47.

Moulin, B., and H. Piégay (2004), Characteristics and temporal variability of large woody debris trapped in a reservoir on the river rhone (rhone): implications for river basin management, *River Research and Applications*, *20*(1), 79–97.

Naiman, R. J., and H. Decamps (1997), The ecology of interfaces: riparian zones, *Annual review of Ecology and Systematics*, *28*(1), 621–658.

Naiman, R. J., R. E. Bilby, and P. A. Bisson (2000), Riparian ecology and management in the pacific coastal rain forest, *BioScience*, *50*(11), 996–1011.

Naiman, R. J., J. S. Bechtold, D. C. Drake, J. J. Latterell, T. C. O'keefe, and E. V. Balian (2005), Origins, patterns, and importance of heterogeneity in riparian systems, in *Ecosystem function in heterogeneous landscapes*, pp. 279–309, Springer.

Nakamura, F., and F. J. Swanson (1993), Effects of coarse woody debris on morphology and sediment storage of a mountain stream system in western oregon, *Earth Surface Processes and Landforms*, *18*(1), 43–61.

Pasquale, N., P. Perona, P. Schneider, J. Shrestha, A. Wombacher, and P. Burlando (2011), Modern comprehensive approach to monitor the morphodynamic evolution of a restored river corridor, *Hydrology and Earth System Sciences*, *15*(4), 1197–1212.

Pasquale, N., P. Perona, R. Francis, and P. Burlando (2014), Above-ground and below-ground salix dynamics in response to river processes, *Hydrological Processes*, *28*(20),

5189–5203.

Perona, P., and B. Crouzy (2018), Resilience of riverbed vegetation to uprooting by flow, *Proceedings of the Royal Society A: Mathematical, Physical and Engineering Sciences*, *474*(2211), 20170,547.

Pinay, G., S. Bernal, B. W. Abbott, A. Lupon, E. Marti, F. Sabater, and S. Krause (2018), Riparian corridors: A new conceptual framework for assessing nitrogen buffering across biomes, *Frontiers in Environmental Science*, *6*, 47.

Pollen, N. (2007), Temporal and spatial variability in root reinforcement of streambanks: accounting for soil shear strength and moisture, *Catena*, *69*(3), 197–205.

Pollen, N., and A. Simon (2005), Estimating the mechanical effects of riparian vegetation on stream bank stability using a fiber bundle model, *Water Resources Research*, *41*(7).

Pollen-Bankhead, N., and A. Simon (2009), Enhanced application of root-reinforcement algorithms for bank-stability modeling, *Earth Surface Processes and Landforms*, *34*(4), 471–480.

Pollen-Bankhead, N., and A. Simon (2010), Hydrologic and hydraulic effects of riparian root networks on streambank stability: Is mechanical root-reinforcement the whole story?, *Geomorphology*, *116*(3-4), 353–362.

Ravazzolo, D., L. Mao, L. Picco, and M. Lenzi (2015), Tracking log displacement during floods in the tagliamento river using rfid and gps tracker devices, *Geomorphology*, *228*, 226–233.

Rigon, E., F. Comiti, and M. Lenzi (2012), Large wood storage in streams of the eastern italian alps and the relevance of hillslope processes, *Water Resources Research*, *48*(1).

Rosso, R., M. C. Rulli, and D. Bocchiola (2007), Transient catchment hydrology after wildfires in a mediterranean basin: runoff, sediment and woody debris, *Hydrology and Earth System Sciences Discussions*, *11*(1), 125–140.

Ruiz Villanueva, V., E. Bladé Castellet, A. Díez-Herrero, J. M. Bodoque, and M. Sánchez-Juny (2014), Two-dimensional modelling of large wood transport during flash floods, *Earth surface processes and landforms*, *39*(4), 438–449.

Ruiz-Villanueva, V., H. Piégay, A. Gurnell, R. A. Marston, and M. Stoffel (2016), Recent advances quantifying the large wood dynamics in river basins: New methods and remaining challenges, *Reviews of Geophysics*, *54*(3), 611–652, doi: 10.1002/2015RG000514.

Ruiz-Villanueva, V., B. Wyżga, J. Zawiejska, P. Mikuś, H. Hajdukiewicz, M. Hajdukiewicz, and M. Stoffel (2016), Large wood transport, deposition and remobilization during floods in the czarny dunajec river: outcomes from numerical modelling, in *Flood Risk in the Upper Vistula Basin*, pp. 103–125, Springer.

Schimpf, D., S. Flint, and I. Palmblad (1977), Representation of germination curves with the logistic function, *Annals of Botany*, *41*(6), 1357–1360.

Schwarz, M., D. Cohen, and D. Or (2011), Pullout tests of root analogs and natural root bundles in soil: Experiments and modeling, *Journal of Geophysical Research: Earth Surface*, *116*(F2).

Sedell, J. R., and J. L. Froggatt (1984), Importance of streamside forests to large rivers: The isolation of the willamette river, oregon, usa, from its floodplain by snagging and streamside forest removal: With 2 figures and 1 table in the text, *Internationale Vereinigung für theoretische und angewandte Limnologie: Verhandlungen*, *22*(3), 1828–1834.

Seo, J. I., and F. Nakamura (2009), Scale-dependent controls upon the fluvial export of large wood from river catchments, *Earth Surface Processes and Landforms*, *34*(6), 786–800.

Smith, F. A. (2007), Plant roots. growth, activity and interaction with soils.

Steiger, J., E. Tabacchi, S. Dufour, D. Corenblit, and J.-L. Peiry (2005), Hydrogeomorphic processes affecting riparian habitat within alluvial channel–floodplain river systems: a review for the temperate zone, *River Research and Applications*, *21*(7), 719–737.

Tabacchi, E., D. L. Correll, R. Hauer, G. Pinay, A.-M. Planty-Tabacchi, and R. C. Wissmar (1998), Development, maintenance and role of riparian vegetation in the river landscape, *Freshwater biology*, *40*(3), 497–516.

Thompson, D. M. (1995), The effects of large organic debris on sediment processes and stream morphology in vermont, *Geomorphology*, *11*(3), 235 – 244, doi: https://doi.org/10.1016/0169-555X(94)00064-X.

Tockner, K., J. V. Ward, D. B. Arscott, P. J. Edwards, J. Kollmann, A. Gurnell, G. E. Petts, and B. Maiolini (2003), The tagliamento river: a model ecosystem of european importance, *Aquatic Sciences*, *65*(3), 239–253.

Trush, W. J., S. M. McBain, and L. B. Leopold (2000), Attributes of an alluvial river and their relation to water policy and management, *Proceedings of the National Academy of Sciences*, *97*(22), 11,858–11,863.

Tyce, G. (1957), Growth substances in relation the the rooting of salix fragilis cuttings, *Annals of Botany*, *21*(3), 499–512.

Ulloa, H., A. Iroumé, L. Picco, O. Korup, M. A. Lenzi, L. Mao, and D. Ravazzolo (2015), Massive biomass flushing despite modest channel response in the rayas river following the 2008 eruption of chaitén volcano, chile, *Geomorphology*, *250*, 397–406.

Welber, M., W. Bertoldi, and M. Tubino (2012), The response of braided planform configuration to flow variations, bed reworking and vegetation: the case of the tagliamento river, italy, *Earth Surface Processes and Landforms*, *37*(5), 572–582.

Welty, J. J., T. Beechie, K. Sullivan, D. M. Hyink, R. E. Bilby, C. Andrus, and G. Pess (2002), Riparian aquatic interaction simulator (rais): a model of riparian forest dynamics for the generation of large woody debris and shade, *Forest Ecology and Management*, *162*(2-3), 299–318.

Wilford, D. J., P. Cherubini, and M. E. Sakals (2005), *Dendroecology: a guide for using trees to date geomorphic and hydrologic events*, British Columbia, Ministry of Forests, Forest Science Program.

Wohl, E. (2011), Threshold-induced complex behavior of wood in mountain streams, *Geology*, *39*(6), 587–590.

Wohl, E. (2019), Forgotten legacies: Understanding and mitigating historical human alterations of river corridors, *Water Resources Research*, *55*(7), 5181–5201, doi: 10.1029/2018WR024433.

Wohl, E., and D. N. Scott (2017), Wood and sediment storage and dynamics in river corridors, *Earth Surface Processes and Landforms*, *42*(1), 5–23.

Wood, D. M. (1990), *Soil behaviour and critical state soil mechanics*, Cambridge university press.

Young, W. J. (1991), Flume study of the hydraulic effects of large woody debris in lowland rivers, *Regulated Rivers: Research & Management*, *6*(3), 203–211, doi: 10.1002/rrr.3450060305.

Zischg, A., N. Galatioto, S. Deplazes, R. Weingartner, and B. Mazzorana (2018), Modelling spatiotemporal dynamics of large wood recruitment, transport, and deposition at the river reach scale during extreme floods, *Water*, *10*(9), 1134.